

Article

Corrosion Investigation of Reinforced Concrete Based on Piezoelectric Smart Materials

Weihua Shi ¹, Ying Chen ^{2,3,*}, Peng Liu ³ and Dongyu Xu ⁴

¹ Hunan Provincial Key Laboratory of Structures for Wind Resistance and Vibration Control & School of Civil Engineering, Hunan University of Science and Technology, Xiangtan 411201, China; llppp98@163.com

² School of Civil Engineering, Central South University of Forestry and Technology, Changsha 410075, China

³ School of Civil Engineering, Central South University, Changsha 410075, China; liupeng868@csu.edu.cn

⁴ Shandong Provincial Key Laboratory of Construction Materials Preparation and Measurement, University of Jinan, Jinan 250022, China; mse_xudy@ujn.edu.cn

* Correspondence: chen83@csu.edu.cn

Received: 12 January 2019; Accepted: 31 January 2019; Published: 9 February 2019



Abstract: An embedded piezoelectric transducer was developed for monitoring the corrosion process of reinforcement bars in concrete based on the piezoelectric impedance technique. The electrochemical method was employed to accelerate the corrosion process of the reinforcement bar with relative mass loss of 0.5–10%, and the resistance spectra of the piezoelectric transducers were investigated to assess the corrosion process. The results show that the corrosion process of the reinforcement bar has significant influence on the resistance spectra of the piezoelectric transducers. Statistical parameters were used to intuitively evaluate the corrosion evolution based on variations of the resistance spectra. The corrosion process of reinforcement bar in concrete can be classified into three periods; that is, the initial period when the relative mass loss is less than 2%, the developing period at a relative mass loss of 2–4%, and the rapid corrosion period when the relative mass loss is higher than 4%.

Keywords: reinforced concrete; piezoelectric; electromechanical; impedance; corrosion

1. Introduction

Concrete is presently a widely utilized construction material in the field of civil engineering, and still will be the most important construction material in the future. However, the concrete structures in service will inevitably be destroyed due to effects of various environmental and natural disasters, thus leading to significant casualties and economic losses. Corrosion of reinforcement bars is one of the most important factors that causes the invalidation of concrete structures [1,2], especially in some coastal construction projects, such as ports, long-span bridges, and offshore drilling platforms. The structural disasters due to corrosion of reinforcement bars in concrete, such as the decrease of structural bearing capacity, expansion cracking of concrete, and deterioration of bonding ability, also appear frequently throughout the world, which has caused extensive concern [3–5]. It is reported that serious steel corrosion exists in the coastal concrete engineering that was constructed before 1990s in China. Therefore, it is an important issue to perform online monitoring on these critical concrete structures to ensure their reliable service.

The corrosion process of reinforcement bars in concrete is an electrochemical process. The passivation film of a reinforcement bar is destroyed by incursion of the external surroundings, and a chemical battery reaction on the steel is accordingly commenced under surroundings of water and oxygen. Effective data are needed to predict the residual life of concrete structures through monitoring the corrosion process of reinforcement bars in concrete. Existing corrosion monitoring techniques can be categorized into analytical methods, physical methods, and electrochemical methods.

The analytical methods [6–8] determine the corrosion extent of reinforcement bars in concrete by building mathematical models in terms of variation of dimension and thickness of the protective layer of the reinforcement bar, concrete strength, and longitudinal crack width, etc. The physical methods employ some advanced materials and facilities to determine the corrosion process by monitoring the physical phenomena in the corrosion process, such as resistance and electromagnetic parameters [9,10] and acoustic and optical wave [11–13]. The electrochemical methods show great potential in monitoring of relative mass loss and extent of reinforcement bars in concrete through variation of electrochemical parameters in the corrosion process [14–16]. Recently, with rapid development of smart materials and structures in the field of civil engineering, some smart materials which are well-used in the fields of aerospace and mechanical engineering have also been transplanted into concrete engineering [17–23]. Among them, piezoelectric materials have gained particular attention due to their merits of fast response time, simple structure, and good reliability. Some online monitoring methods based on piezoelectric transducers have also been developed, such as the piezoelectric strain technique, ultrasonic technique, and piezoelectric impedance technique [17,24–26].

It is known that the mechanical characteristics of reinforcement bars in concrete, such as stiffness and damping, will change when suffering from corrosion. If piezoelectric transducers are coupled with concrete, the mechanical impedance of the corroded reinforcement bar will affect the electric impedance versus frequency spectra of the piezoelectric transducers [27,28]. Therefore, a kind of piezoelectric impedance technique was proposed in this study to monitor the corrosion process of reinforcement bars in concrete by developing a kind of embedded piezoelectric transducer.

2. Experiments

2.1. Principle of the Piezoelectric Impedance Technique

Figure 1 shows the one-dimensional interaction model between the piezoelectric transducer and host structure, in which the host structure can be regarded as a system of the spring ($k1$)-mass ($m1$)-damper ($c1$) model.

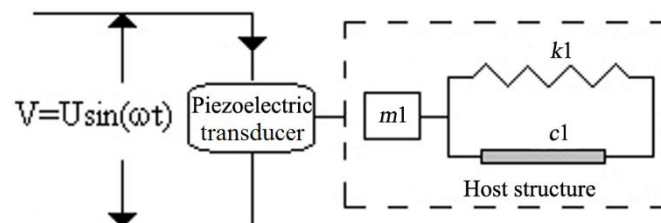


Figure 1. One-dimensional interaction model of the piezoelectric transducer and host structure. V : the instantaneous voltage; U : maximum value of voltage; ω : angular frequency; t : time; $c1$: damper; $k1$: spring; $m1$: mass.

It is known based on the theoretical model proposed by Liang et al. [24] that the electrical admittance $Y(\omega)$ of a piezoelectric transducer is a combined function of the mechanical impedance $Z_a(\omega)$ of piezoelectric transducer and the $Z(\omega)$ of the host structure:

$$Y(\omega) = \frac{I}{V} = i\omega a(\varepsilon_{33}^T - \frac{Z(\omega)}{Z(\omega) + Z_a(\omega)} d_{3x}^2 Y_{xx}^E) \quad (1)$$

where V is the input voltage of piezoelectric transducer, I is the output current from the transducer, and a , d_{3x} , Y_{xx}^E , and ε_{33}^T are the geometry constant, piezoelectric coupling constant, complex Young's modulus at zero electric field, and complex dielectric constant of the piezoelectric transducer at zero stress, respectively.

The electrical impedance of a piezoelectric transducer is related to the mechanical impedance of the host structure in this equation, and any changes of electrical impedance of the piezoelectric

transducers can be considered as an indication of the structural integrity. Thus, the damage condition of the host structure can be monitored by analyzing the variation of electric impedance of the piezoelectric transducer.

2.2. Corrosion Experiment of the Reinforcement Bar in Concrete

Two PZT (Lead Zirconate Titanate) wafers of $\Phi 12 \times 2 \text{ mm}^2$ (#1) and $\Phi 12 \times 5 \text{ mm}^2$ (#2) were used to fabricate the piezoelectric transducers, as shown in Figure 2a. First, the shielding wires were welded to both electrodes of the wafers, and then cement, epoxy resin, and hardening agent were mixed together to encapsulate the PZT wafers with a mass ratio of 1:1:0.25. Before packaging, the mixture was first put into the vacuum chamber for 5 min to reduce the air pores, and a thin layer of the mixture of $1 \pm 0.2 \text{ mm}$ in thickness was then coated on both PZT wafers and the exposed parts of the wires, as shown in Figure 2b. After solidifying of the packaging layer, the PZT transducers were tested in water to ensure their reliability in a practical monitoring application.



Figure 2. Photographs of the piezoelectric transducer and corroded reinforced concrete. (a) PZT (Lead Zirconate Titanate) wafers; (b) Piezoelectric transducers; (c) Steel bar attached a transducer; (d) Corroded reinforced concrete.

Here, a round steel bar of $\Phi 14 \times 340 \text{ mm}^2$ was monitored, and the mixture of cement, epoxy resin, and hardening agent mentioned above was used to stick PZT transducers to both ends of the steel bar. In addition, a wire was also welded to the middle part of the steel bar to connect the electrochemical workstation, as shown in Figure 2c. The C30 concrete was designed with a mass ratio of cement/sand/stone/water of 1:2.2:3.6:0.6. The corrosion process of steel in a natural environment is a slow process; therefore, the accelerated corrosion of reinforced concrete was performed by using the electrochemical workstation, as shown in Figure 3. The concrete block was placed in a container with 5% NaCl solution. Stainless steel was used as the auxiliary electrode of the electrochemical workstation, and the reinforcement bar in concrete was used as working electrode. The current density was maintained at 1 mA cm^{-2} . The impedance analyzer was employed to acquire the electric impedance data of PZT transducers.

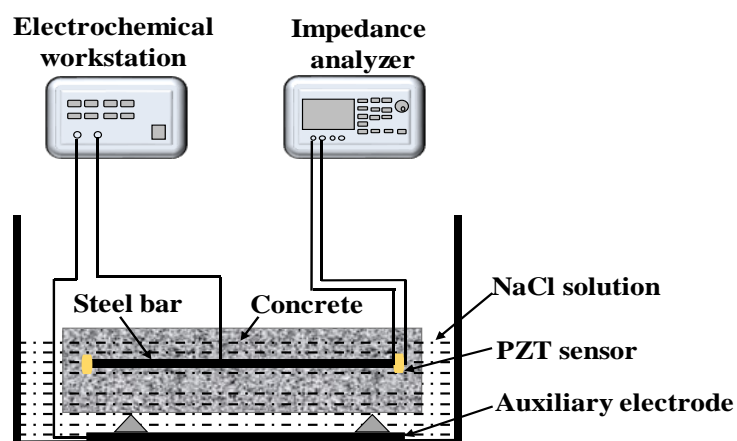
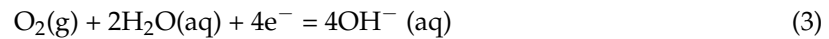


Figure 3. Schematic diagram of corrosion monitoring of reinforced concrete.

Based on the electrochemical corrosion principle, it is known that an oxidation–reduction reaction exists in the electrochemical corrosion process of steel. The reaction is usually expressed as follows:



The relative mass loss of steel can be controlled by changing the current intensity, and the corrosion mass of steel can then be obtained theoretically according to Faraday's laws, as shown in Equation (4). The relative mass loss (Δv) was calculated based on the mass loss rate of reinforcement bar before and after corrosion, as shown in Equation (5).

$$\Delta m = n \cdot M = \frac{Q \cdot M}{F \cdot |Z|} = \frac{M \int I(t) dt}{F \cdot |Z|} \quad (4)$$

$$\Delta v = \frac{\Delta m}{m} \quad (5)$$

where Δm is the mass of steel being corroded, m is the mass of steel before corrosion, Q is the quantity of electric charge, F is the Faraday constant, $I(t)$ and t are the current intensity and time, $|Z|$ is the absolute value of valence of ferric iron, n is the amount of substance of the corroded steel, and M is the molar mass of iron.

2.3. Electric Impedance Test of PZT Transducers

The electric impedance spectra of PZT transducers were recorded by the precision impedance analyzer. According to the monitoring principle of the piezoelectric impedance technique, the variation of mechanical impedance of steel in concrete can be obtained by analyzing the electric impedance variation of PZT transducers. Here, concrete cured in standard conditions (temperature: 20 ± 2 °C, relative humidity: $\geq 95\%$) for 28 days was regarded as the pristine state of the corrosion process, and the electric impedance value at this state was used as baseline. The electric impedance spectra of PZT transducers were tested in a frequency range of 40–800 kHz. In order to improve the monitoring resolution, the tested frequency range was divided into 32 frequency intervals, and there were 801 frequency points in every frequency interval. The electrochemical workstation was employed to control the current intensity and duration of polarization based on Faraday's laws, and the electric impedance data were recorded every 0.5% until a relative mass loss of 10% was reached.

3. Results and Discussion

3.1. Impedance Spectra Comparison of PZT Transducers before and after Packaging

It is well known that piezoelectric materials vibrate under excitation of alternating current due to the converse piezoelectric effect, and the resonant phenomena can usually be observed from the impedance spectra. According to the principle of the piezoelectric impedance technique, the impedance spectra of PZT transducers with packaging layer will be different from that without the packaging layer; therefore, the mechanical impedance variation of the coupled structure can be indicated based on this impedance variation of PZT transducers.

Figure 4 presents the resistance and reactance of PZT transducers before and after packaging. There exist a series of resonant peaks in a frequency range of 40–800 kHz, especially in the resistance spectra. The frequencies of the dominant resonant peaks are about 200 kHz for PZT transducer #1 and 180 kHz for PZT transducer #2. After packaging, it can be clearly observed that the amplitude of the resonant peaks decreases sharply and some weak resonant peaks even disappear, while some new resonant peaks also appear.

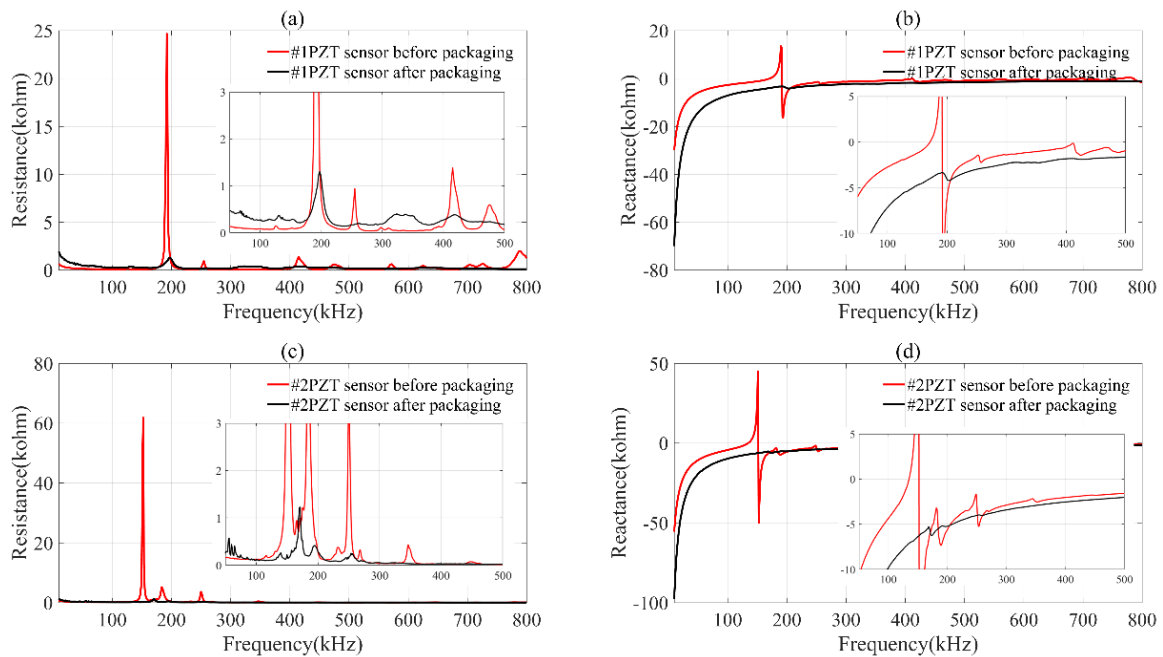


Figure 4. The resistance and reactance spectra of PZT transducers before and after packaging. (a) resistance spectra of 1#PZT sensor before and after packaging; (b) reactance spectra of 1#PZT sensor before and after packaging; (c) resistance spectra of 2#PZT sensor before and after packaging; (d) reactance spectra of 2#PZT sensor before and after packaging.

The variation of resonant peaks shows that the packaging layer has influence on impedance spectra of the PZT transducer. The basic equivalent circuit of piezoelectric material around the resonant frequency is illustrated in Figure 5 [24,26].

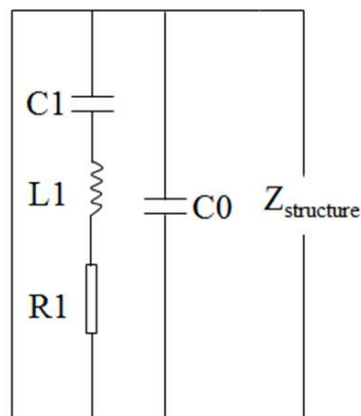


Figure 5. Equivalent circuit of piezoelectric materials around the resonant frequency. C_0 : the parallel capacitance; R_1 : dynamic electric resistivity; C_1 : dynamic electric capacitance; L_1 : dynamic electric inductance

In Figure 5, the dynamic electric parameters are consisted of resistivity R_1 , capacitance C_1 and inductance L_1 , which are associated with the coupled load (i.e., packaging layer). The resonant ability of the PZT transducer weakens under the effects of mechanical damping of the packaging layer, and thus the electric impedance of the transducer changes correspondingly.

3.2. Impedance Spectra of PZT Transducers under Different Relative Mass Losses

Through comparing the resistance versus frequency spectra in different frequency intervals, it can be found that the resonant peaks of PZT transducers appear mainly in the frequency range of

20–500 kHz. In this study, the typical resistance versus frequency spectra in two different frequency intervals for both PZT transducers were analyzed.

Figure 6 shows the resistance versus frequency spectra of both PZT transducers in a frequency range of 25–75 kHz. As the relative mass loss increases, it can be observed that the resistance versus frequency curves show obvious variation, such as drifts of resonant frequency, amplitude variation of resistance, and variation in amounts of the resonant peaks. When the relative mass loss is less than 1%, the variation of resistance spectra for both PZT transducers is not obvious; that is, the weak corrosion just causes a slight resistance variation. When the relative mass loss is higher than 1%, the resistance value and the resonant frequency of the spectra have obvious variation. As the relative mass loss increases, some new resonant peaks can also be clearly observed, especially in the spectra of PZT transducer #1.

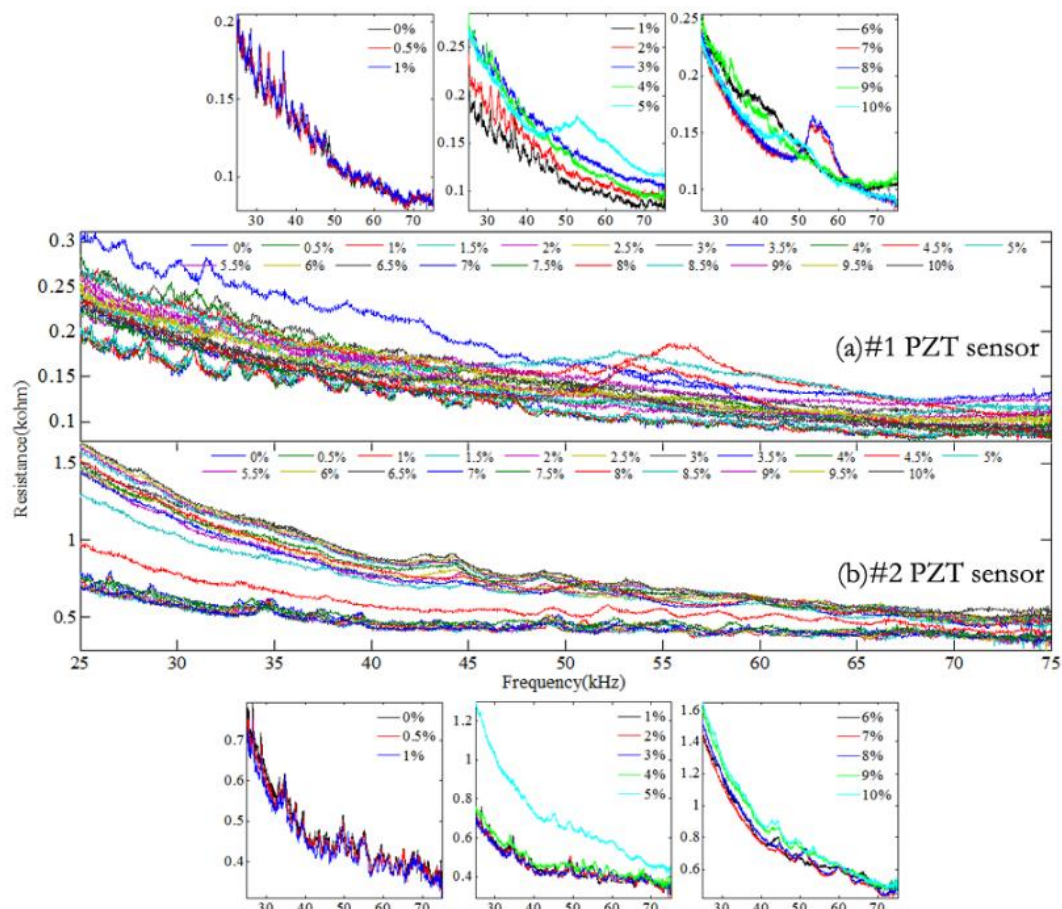


Figure 6. Resistance vs. frequency spectra for PZT transducers in the frequency range of 25–75 kHz.

The dominant resonant frequencies of PZT transducers #1 and #2 appear in the frequency range of 150–200 kHz and 125–175 kHz, respectively. The resistance versus frequency spectra of both PZT transducers in this frequency interval are shown in Figure 7. It can be seen that the dominant resonant peaks of both PZT transducers shift obviously with increasing the relative mass loss. Compared with Figure 6, the variation of the resistance curve is more obvious as the relative mass loss increases, even though the relative mass loss is small.

Through investigating the resistance versus frequency spectra, the conclusion can be drawn that the spectra are greatly influenced by the mechanical impedance variation of corroded steel. As the relative mass loss increases, the frequency of the resonant peaks shifts and the amplitude of the resonant peak changes. Compared with Figure 6, the resistance versus frequency spectra in Figure 7

which contains the dominant resonant peaks of PZT transducers has a better ability to identify the initial corrosion of reinforced concrete.

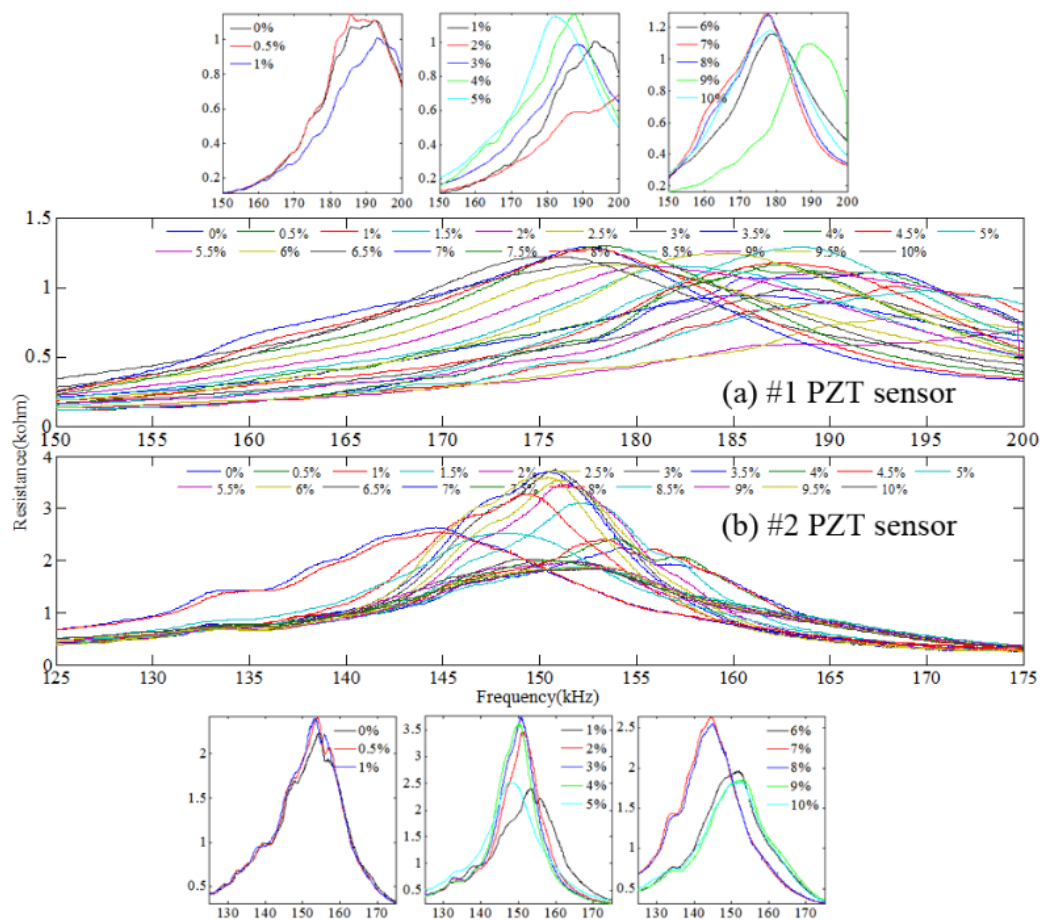


Figure 7. Resistance vs. frequency spectra of PZT transducers in different frequency intervals.

3.3. Statistical Analysis of Impedance Spectra

The corrosion variation of steel in concrete can be observed through the resistance versus frequency spectra of PZT transducers; however, the variation law of the corrosion process cannot be obtained intuitively from the spectra. Therefore, appropriate quantitative damage indices are important to evaluate the corrosion process of reinforcement concrete. Here, the statistical method was used to analyze the variation of resistance versus frequency spectra of PZT transducers. The mathematical models of root mean square deviation (RMSD), mean absolute percentage deviation (MAPD), and correlation coefficient (CC) were established as the corrosion indices.

$$CC = \frac{1}{n\sigma_{R_i^0}\sigma_{R_i}} \sum_{i=1}^n (R_i^0 - \bar{R}_i^0)(R_i - \bar{R}_i) \tag{6}$$

$$RMSD = \sqrt{\frac{\sum_{i=1}^n [|R_i| - |R_i^0|]^2}{\sum_{i=1}^n [|R_i^0|]^2}} \tag{7}$$

$$MAPD = \frac{1}{n} \sum_{i=1}^n \left| \frac{R_i - R_i^0}{R_i^0} \right| \tag{8}$$

where $|R_i|$ is the resistance value of PZT transducers in the spectra, $|R_i^0|$ is the reference resistance value of PZT transducers when the relative mass loss is 0%, and n is the frequency count in the spectra.

The corrosion indices were calculated based on the resistance versus frequency spectra of PZT transducers in Figure 6, as shown in Figure 8. It can be observed that when the relative mass loss is less than 4%, the CC index presents a slow downward trend, but the RMSD and MAPD indices show the increasing trend, especially for PZT transducer #1. A transition exists at a relative mass loss of about 2%, and as the relative mass loss increases, the CC index decreases evidently and the RMSD and MAPD indices increase remarkably. When the relative mass loss is higher than 4%, the CC index of PZT transducer #1 shows a fluctuating variation, but that of PZT transducer #2 shows a decreasing trend. The RMSD and MAPD indices have a similar variation for PZT transducer #1, which decrease evidently as the relative mass loss increases. On the contrary, the RMSD and MAPD indices of PZT transducer #2 increase greatly as the relative mass loss increases.

In addition, the corrosion indices were also calculated based on the resistance versus frequency spectra of PZT transducers in Figure 7, as shown in Figure 9. It can be seen that when the relative mass loss is less than 4%, the CC index decreases gradually as the relative mass loss increases, while the RMSD and MAPD indices show an increasing trend, especially for PZT transducer #2. A transition also exists at a relative mass loss about 2%. When the relative mass loss is higher than 4%, all the corrosion indices show obvious fluctuation. This phenomenon indicates that there has been a violent corrosion reaction of the steel in the concrete; therefore, the resistance of PZT transducers changes greatly because of variation of the mechanical impedance of the corroded steel.

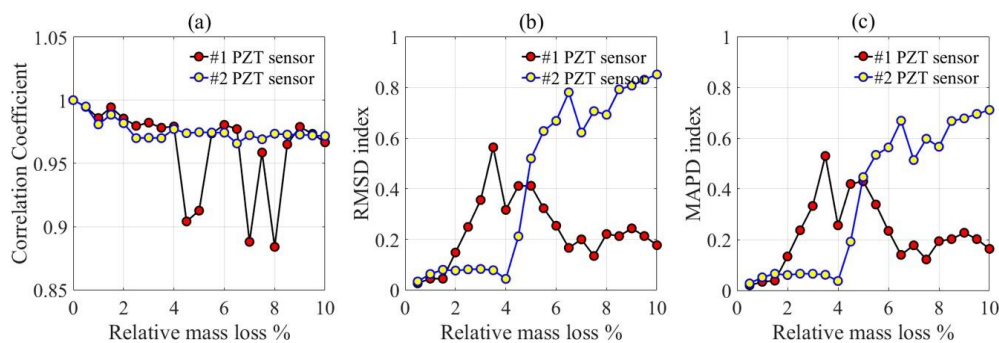


Figure 8. Corrosion indices of PZT transducers in a frequency interval of 25–75 kHz. (a) Correlation Coefficient; (b) RMSD index; (c) MAPD index. RMSD: root mean square deviation; MAPD: mean absolute percentage deviation.

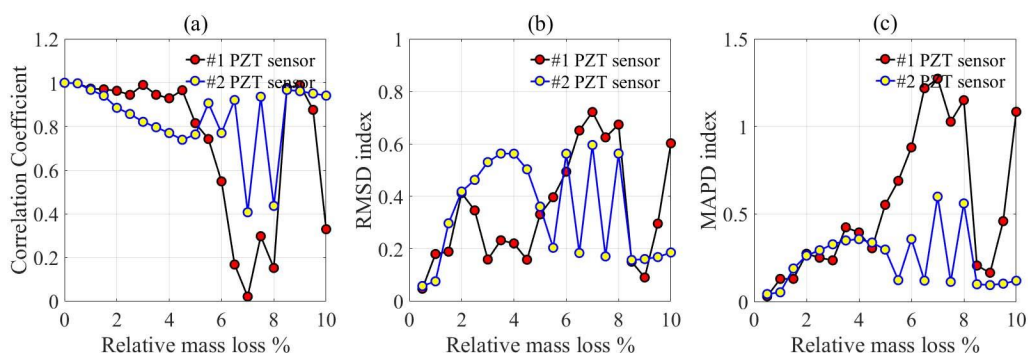


Figure 9. Corrosion indices of PZT transducers in a frequency interval of 150–200 kHz for transducer #1 and 125–175 kHz for transducer #2. (a) Correlation Coefficient; (b) RMSD index; (c) MAPD index.

Based on the corrosion indices, the corrosion behavior of the reinforcement concrete can be categorized into the following periods: Firstly, the initial corrosion period when the relative mass loss is less than 2%. There is a smooth variation of corrosion indices in this period. Secondly, the increasing corrosion period when the relative mass loss is between 2% and 4%. There is an obvious variation of

corrosion indices in this period. Finally, the rapidly developing period when the relative mass loss is higher than 4%; obvious fluctuation of corrosion indices is exhibited in this period.

4. Conclusions

PZT ceramic was used as a piezoelectric element, and a mixture of cement, epoxy resin, and hardening agent was used as an encapsulating material to fabricate the embedded piezoelectric transducers. The piezoelectric impedance technique was employed to evaluate the corrosion process of reinforced concrete. As the relative mass loss increases, the resistance spectra of the piezoelectric transducers show obvious variation. The root mean square deviation (RMSD), mean absolute percentage deviation (MAPD), and correlation coefficient (CC) were established to evaluate the corrosion process of reinforced concrete, and three corrosion periods can be concluded based on these parameters; that is, the initial corrosion period when the relative mass loss is less than 2%, the increasing corrosion period when the relative mass loss is about 2–4%, and the rapidly developing period when the relative mass loss is higher than 4%.

Author Contributions: Conceptualization, P.L. and D.X.; methodology, Y.C.; software, W.S.; validation, W.S., Y.C. and D.X.; formal analysis, P.L.; investigation, W.S., Y.C. and D.X.; resources, W.S.; data curation, D.X.; writing—original draft preparation, W.S.; writing—review and editing, Y.C.; visualization, Y.C.; supervision, D.X.; project administration, P.L. and D.X.; funding acquisition, P.L. and D.X.

Funding: This work was supported by National Natural Science Foundation of China (grant No. 51678234, No. 51778632, No. 51408614, and No. U1434204), the National Key Research and Development Program of China (grant No. 2017YFE0120900), the Hunan Provincial Natural Science Foundation of China (grant No. 2015JJ2069 and No. 2017JJ3385), the China Postdoctoral Science Foundation (grant No. 2016M600675 and No. 2017T100647), and the Basic Research on Science and Technology Program of Shenzhen (JCYJ20170818143541342).

Conflicts of Interest: The authors declare no conflict of interest.

References

1. Metha, P.K. Durability-critical issues for the future. *Conc. Int.* **1997**, *19*, 27–33.
2. Cabrera, J.G. Deterioration of concrete due to reinforcement steel corrosion. *Cement Conc. Comp.* **1996**, *18*, 47–59. [[CrossRef](#)]
3. Ahmad, S. Reinforcement corrosion in concrete structures, its monitoring and service life prediction—a review. *Cement Conc. Comp.* **2003**, *25*, 459–471. [[CrossRef](#)]
4. Raupach, M. Chloride-induced macrocell corrosion of steel in concrete—theoretical background and practical consequences. *Constr. Build. Mater.* **1996**, *10*, 329–338. [[CrossRef](#)]
5. Bertolini, L.; Gastaldi, M.; Pedeferri, M.P.; Redaelli, E. Prevention of steel corrosion in concrete exposed to seawater with submerged sacrificial anodes. *Corros. Sci.* **2002**, *44*, 1497–1513. [[CrossRef](#)]
6. Isgor, O.B.; Razaqpur, A.G. Modelling steel corrosion in concrete structures. *Mater. Struct.* **2006**, *39*, 291–302. [[CrossRef](#)]
7. Jung, W.Y.; Yoon, Y.S.; Sohn, Y.M. Predicting the remaining service life of land concrete by steel corrosion. *Cement Conc. Res.* **2003**, *33*, 663–677. [[CrossRef](#)]
8. Kranc, S.C.; Sagüés, A.A. Computation of reinforcing steel corrosion distribution in concrete marine bridge substructures. *Corrosion* **1994**, *50*, 50–61. [[CrossRef](#)]
9. Gonzalez, J.A.; Feliu, S.; Andrade, M.C. Confinement of electrical signal for in-situ measurement of polarization resistance in reinforced concrete. *ACI Mater. J.* **1990**, *87*, 457–460.
10. Gaydecki, P.; Fernandes, B.; Quek, S.; Benitez, D.; Miller, G.; Zaid, M. Inductive and magnetic field inspection systems for rebar visualization and corrosion estimation in reinforced and pre-stressed concrete. *Nondestruct. Test. Eva.* **2007**, *22*, 255–298. [[CrossRef](#)]
11. Idrissi, H.; Limam, A. Study and characterization by acoustic emission and electrochemical measurements of concrete deterioration caused by reinforcement steel corrosion. *NDT E Int.* **2003**, *36*, 563–569. [[CrossRef](#)]
12. Weng, M.S.; Dunn, S.E.; Hartt, W.H.; Brown, R.P. Application of acoustic emission to detection of reinforcing steel corrosion in concrete. *Corrosion* **1982**, *38*, 9–14. [[CrossRef](#)]
13. Fuhr, P.L.; Huston, D.R. Corrosion detection in reinforced concrete roadways and bridges via embedded fiber optic sensors. *Smart Mater. Struct.* **1998**, *7*, 217–228. [[CrossRef](#)]

14. Bertolini, L.; Carsana, M.; Pedefferri, P. Corrosion behaviour of steel in concrete in the presence of stray current. *Corros. Sci.* **2007**, *49*, 1056–1068. [[CrossRef](#)]
15. Hussaina, R.R.; Ishidab, T. Enhanced electro-chemical corrosion model for reinforced concrete under severe coupled action of chloride and temperature. *Constr. Build. Mater.* **2011**, *25*, 1305–1315. [[CrossRef](#)]
16. Chen, W.; Du, R.G.; Ye, C.Q.; Zhu, Y.F.; Lin, C.J. Study on the corrosion behavior of reinforcing steel in simulated concrete pore solutions using in situ Raman spectroscopy assisted by electrochemical techniques. *Electrochim. Acta* **2010**, *55*, 5677–5682. [[CrossRef](#)]
17. Song, G.; Gu, H.; Mo, Y.L.; Hsu, T.T.C.; Dhonde, H. Concrete structural health monitoring using embedded piezoceramic transducers. *Smart Mater. Strut.* **2007**, *16*, 959–968. [[CrossRef](#)]
18. Lau, K.; Yuan, L.; Zhou, L.; Wu, J.; Woo, C. Strain monitoring in FRP laminates and concrete beams using FBG sensors. *Compos. Struct.* **2001**, *51*, 9–20. [[CrossRef](#)]
19. Lee, H.K.; Lee, K.M.; Kim, Y.H.; Yim, H.; Bae, D.B. Ultrasonic in-situ monitoring of setting process of high-performance concrete. *Cement Conc. Res.* **2004**, *34*, 631–640. [[CrossRef](#)]
20. Shin, S.W.; Oh, T.K. Application of electro-mechanical impedance sensing technique for online monitoring of strength development in concrete using smart PZT patches. *Constr. Build. Mater.* **2009**, *23*, 1185–1188. [[CrossRef](#)]
21. Inci, P.; Goksu, C.; Ilki, A.; Kumbasar, N. Effects of reinforcement corrosion on the performance of RC frame buildings subjected to seismic actions. *J. Perform. Constr. Fac.* **2012**, *27*, 683–696. [[CrossRef](#)]
22. Goksu, C.; Ilki, A. Seismic behavior of reinforced concrete columns with corroded deformed reinforcing bars. *ACI Struct. J.* **2016**, *113*, 1053–1064.
23. Zhang, D.; Zhao, Y.; Jin, W.; Ueda, T.; Nakai, H. Shear strengthening of corroded reinforced concrete columns using pet fiber based composites. *Eng. Struct.* **2017**, *153*, 757–765. [[CrossRef](#)]
24. Tracy, M.; Chang, F.K. Identifying impacts in composite plates with piezoelectric strain sensors, Part II: Experiment. *J. Intel. Mat. Syst. Strut.* **1998**, *9*, 929–937. [[CrossRef](#)]
25. Soh, C.K.; Bhalla, S. Calibration of piezo-impedance transducers for strength prediction and damage assessment of concrete. *Smart Mater. Strut.* **2005**, *14*, 671–684. [[CrossRef](#)]
26. Liang, C.; Sun, F.P.; Rogers, C.A. Electro-mechanical impedance modeling of active material systems. *J. Intel. Mater. Syst. Strut.* **1994**, *21*, 232–252. [[CrossRef](#)]
27. Giurgiutiu, V.; Zagrai, A.; Bao, J.J. Piezoelectric wafer embedded active sensors for aging aircraft structural health monitoring. *Struct. Health. Monit.* **2002**, *1*, 41–61. [[CrossRef](#)]
28. Xu, D.Y.; Huang, S.F.; Cheng, X. Electromechanical impedance spectra investigation of impedance-based PZT and cement/polymer based piezoelectric composite sensors. *Constr. Build. Mater.* **2014**, *65*, 543–550. [[CrossRef](#)]

